DIFFUSE-INTERFACE SIMULATIONS OF CAPILLARY PHENOMENA

Walter Villanueva

June 2007 Technical Reports from Royal Institute of Technology Department of Mechanics SE-100 44 Stockholm, Sweden

Akademisk avhandling som med tillstånd av Kungliga Tekniska Högskolan i Stockholm framlägges till offentlig granskning för avläggande av teknologie doktorsexamen fredagen den 8 june 2007 kl. 10.00 i Sal F2 Kungliga Tekniska Högskolan, Lindstedtsvägen 26, Stockholm. © Walter Villanueva 2007

Universitetsservice US AB, Stockholm 2004



DIFFUSE-INTERFACE SIMULATIONS OF CAPILLARY PHENOMENA

Walter Villanueva 2007

Department of Mechanics, Royal Institute of Technology SE-100 44 Stockholm, Sweden.

Abstract

Fluid flows mainly driven by capillary forces are presented in this thesis. By means of modeling and simulations, interesting dynamics in capillary-driven flows are revealed such as coalescences, breakups, precursor films, flow instabilities, rapid spreading, rigid body motions, and reactive wetting.

Diffuse-interface methods model a fluid interface as having a finite thickness endowed with physical properties such as surface tension. Two diffuse-interface models that are based on the free energy of the system are presented. The binary model, more specifically the coupled Navier-Stokes/Cahn-Hilliard equations, was used to study different two-phase flows including problems related to microfluidics. Numerical issues using this model have been addressed such as the need for mesh adaptivity and time-step restrictions. Moreover, the flexibility of this model to simulate 2D, axisymmetric, and 3D flows has been demonstrated.

The factors affecting reproducibility of microdroplet depositions performed under a liquid medium are investigated. In the deposition procedure, sample solution is dispensed from the end of a capillary by the aid of a pressure pulse onto a substrate with pillar-shaped sample anchors. In both the experimental and numerical study it was shown that the deposited volume mainly depends on the capillary-substrate distance and anchor surface wettability. Furthermore, a critical equilibrium contact angle has been identified below which reproducible depositions are facilitated.

The ternary model is developed for more complicated flows such as liquid phase sintering. With the introduction of a Gibbs energy functional, the governing equations are derived, consisting of convective concentration and phase-field equations which are coupled to the Navier-Stokes equations with surface tension forces. Arbitrary phase diagrams, surface energies, and typical dimensionless numbers are some input parameters into the model. Detailed analysis of the important capillary phenomena in liquid phase sintering such as reactive and nonreactive wetting and motion of two particles connected by a liquid bridge are presented. The dynamics of the wetting is found to match with a known hydrodynamic theory for spreading liquids. Factors affecting the equilibrium configuration of the particles such as equilibrium contact angles and volume ratios are also investigated.

Descriptors: capillary-driven flows, wetting, Cahn-Hilliard/Navier-Stokes system, multicomponent and multiphase flows, parallel adaptive computing, diffuse-interface, phase-field method, liquid phase sintering, microfluidics.

Preface

This thesis pertains to the study of capillary phenomena at the microscale. In the first part, a short introduction to the basic concepts, theories, applications, and methods within the field is presented. The intention of the author is to provide basic relevant information that complements the papers which are presented in the second part of this thesis, as well as list some references for further reading. The second part consists of the following papers:

- **Paper 1.** Villanueva, W. and Amberg, G. 2006 Some generic capillary-driven flows. *Int. J. Multiphase Flow*, **32**, p.1072-1086.
- **Paper 2.** Villanueva, W., Sjödahl, J., Stjernström, M., Roeraade, J., and Amberg, G. 2007 Microdroplet deposition under a liquid medium. *Langmuir*, **23** (3), p.1171-1177.
- **Paper 3.** Do-Quang, M., Villanueva, W., Singer-Loginova, I., and Amberg G. 2007 Parallel adaptive computation of some time-dependent materials-related microstructural problems. *Bulletin of the Polish Academy of Sciences*, to appear.
- **Paper 4.** Villanueva, W., Grönhagen, K., Amberg, G., and Ågren, J. 2007 Multi-component and multiphase modeling and simulation of reactive wetting. Submitted to *Physical Review E*.
- **Paper 5.** Villanueva, W., Grönhagen, K., Amberg, G., and Ågren, J. 2007 Multicomponent and multiphase simulations of liquid phase sintering. To be submitted.

Paper not included in this thesis:

Villanueva, W. and Amberg, G. 2006 Phase-field simulations of free boundary microflows. *Proceedings of the 2nd Int. Conf. on Transport Phenomena in Micro and Nanodevices*. Barga, Italy.

Division of work between paper authors

- **Paper 1.** The respondent performed the simulations with guidance from Gustav Amberg (GA). The respondent wrote the paper with input from GA.
- Paper 2. The problem was suggested by Johan Roeraade and GA. The respondent performed the simulations with guidance from GA. Johan Sjödahl (JS) performed the experiments with feedback from all authors. The respondent analysed the data and wrote the paper with input from JS on the experimental part, and feedback from all authors.
- **Paper 3.** The parallel adaptive scheme was coded and verified by Minh Do-Quang (MD) and wrote the dendritic growth part with input from Irina Singer-Loginova. The respondent performed the capillary-driven flows and wrote this part. The respondent was responsible for the literature reviews and documentation of the paper with guidance from MD and feedback from GA.
- **Paper 4.** The model was based on previous works of all authors. The respondent nondimensionalised the model with input from Klara Grönhagen (KG). The simulations were performed by the respondent with input from KG and feedback from GA and John Ågren (JÅ). The respondent was responsible for the writing with input from KG and feedback from GA and JÅ.
- **Paper 5.** The model used is similar to Paper 4. The simulations were performed by the respondent with input from KG and feedback from GA and JÅ. The respondent was responsible for the writing with input from KG and feedback from GA and JÅ.

Contents

Preface	vii
Chapter 1. Basic concepts 1.1. Surface tension 1.2. Wetting	1 1 2
Chapter 2. Applications	5
2.1. Liquid phase sintering	5
2.2. Microfluidics	6
Chapter 3. Mathematical modeling	9
3.1. Modeling wetting	9
3.2. Diffuse-interface methods	10
3.3. Navier-Stokes flow	13
Chapter 4. Computational aspects	15
4.1. Numerical treatment	15
4.2. Finite element discretisation	15
4.3. Parallel adaptive computation	19
Chapter 5. Summary of results	20
Chapter 6. Conclusions and outlook	27
Acknowledgment	29
Bibliography	30

Part 1 Introduction and Summary

CHAPTER 1

Basic concepts

1.1. Surface tension

The concept of surface tension can be viewed in two ways. It can be thought of as a force per unit length or a surface free energy per unit area (Probstein 2003; Adamson 1990).

Consider a liquid-gas system forming an interface, see Fig. 1.1. Molecules sense and interact with each other. A molecule in the bulk liquid is attracted by all neighbouring molecules from all directions. Any attraction by another molecule from one direction is always balanced by another molecule from the opposite direction. On the other hand, a molecule on the interface is attracted inward and to the side but no outward attraction to balance the inward attraction since there are not so many molecules outside in the gas. This unbalanced attraction will tend the surface to contract. Surface tension effects can be observed in many commonplace phenomena such as drops formed by liquids in air or in another liquid, thin films and coatings, liquid jets, and capillary rise. For discussions on the molecular causes of capillarity, see (Rowlinson & Widom 1982; Israelachvili 1992).

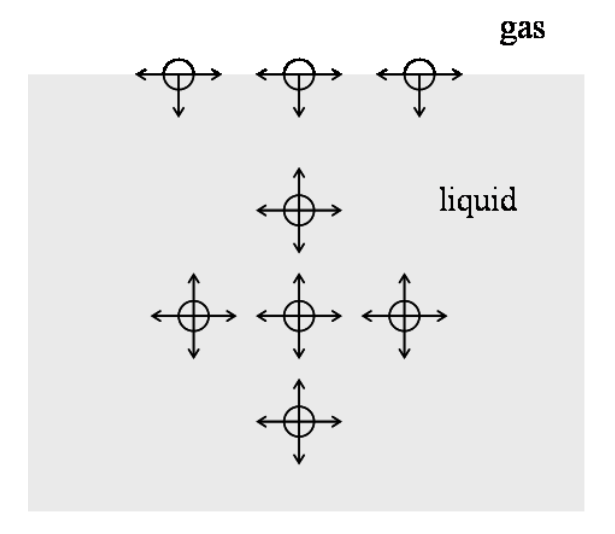


FIGURE 1.1. Molecular interactions at the interface and in the bulk liquid for a plane liquid-gas interface.

The term surface free energy is also being used interchangeably with surface tension. This stems from the fact that the energy of a molecule at the surface is higher than that of a molecule in the bulk liquid. So, a 'wandering' molecule

2 1. BASIC CONCEPTS

would then increase the free energy of the system if it moves to the surface coming from the interior, and decrease the system's free energy if it does otherwise. Since the free energy of the system must tend to a minimum, the surface will tend to contract, exposing its least possible surface area.

The units of surface tension is usually given in force per unit length, and equivalently, energy per unit area. Typical values are: water-vapor, $72.94 \, mN/m$, ethanol-vapor, $22.39 \, mN/m$, and mercury-vapor, $486.5 \, mN/m$, all at 20° C (Adamson 1990).

Surface tension depends on temperature and it decreases as the liquid temperature increases. Moreover, surface tension could also be altered by surface-active materials, termed surfactants, that creates a monolayer at the surface. It can be shown, using the Gibbs equation that there is a decrease in surface tension with an increase in concentration of surfactants adsorbed at the interface (for more discussions, see Adamson 1990; Probstein 2003).

1.2. Wetting

When a fluid/fluid interface makes a contact with a third phase, usually a solid surface, we have a phenomenon called wetting. It is widespread in physical and biological sciences such as the rise of sap in plants (which is a vital subprocess in photosynthesis), penetration of liquids into porous rock, and many others.

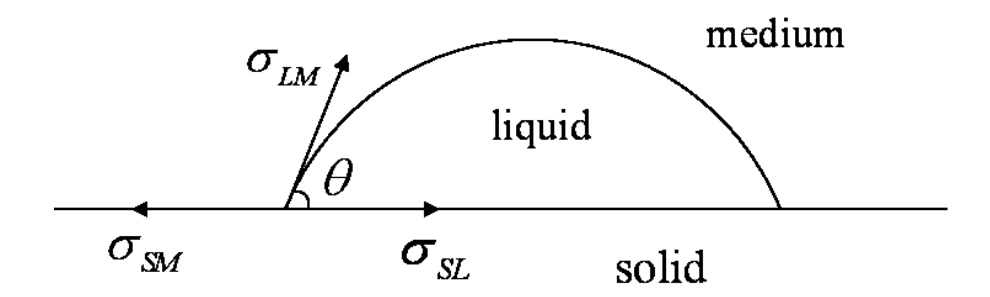


FIGURE 1.2. Wetting of a liquid drop on a solid surface.

The wetting of a liquid on a solid surface can be classified into two types (de Gennes et al. 2004): total wetting, when the liquid spreads completely; and partial wetting, when the liquid at equilibrium rests on the solid with a contact angle θ_e , see Fig. 1.2. Both are characterized by the spreading parameter $S = \sigma_{SM} - (\sigma_{SL} + \sigma_{LM})$, where the σ 's are surface tensions at the solid/medium (medium is either air or another liquid), solid/liquid, liquid/medium interfaces, respectively. S > 0 corresponds to total wetting and S < 0 corresponds to partial wetting. High-energy surfaces such as metallic surfaces has higher σ_{SM} values, thus increases S, compared to low-energy surfaces such as plastics. Wettability can also be controlled through surface roughness and surface coatings. Surface roughness enhances wetting when the surface is hydrophilic and the opposite if the

surface is hydrophobic. Examples of superhydrophobic surfaces include bird feathers and lotus leaves that have equilibrium contact angles of 150 and 170 degrees, respectively.

There is a relation between the static equilibrium contact angle θ_e and the interfacial tensions (see Fig. 1.2), and this is given by the Young's equation (Young 1805),

$$\cos \theta_e = \frac{\sigma_{SM} - \sigma_{SL}}{\sigma_{LM}} \tag{1.1}$$

with the assumption that S < 0 and the solid surface remains rigid and smooth. For a solid surface that is rough or has impurities, the static contact angle may not be unique but lies between the static advanced and receded contact angles (Johnson & Dettre 1964). This is called the contact-angle hysteresis.

The quantity $k = \cos \theta_e$ is often referred to as the wetting coefficient. This quantity when plotted against the surface tension σ_{LM} (of different alkanes) gives the Zisman plot (Zisman 1964). It is useful in the determination of critical surface tension of different surfaces which is related to their wettabilities.

Another important concept in the study of wetting is the dynamic contact angle. To illustrate this, let us start with a liquid drop spreading on a smooth solid surface. As the wetting line moves, the contact angle changes approaching a stable value which is the equilibrium contact angle θ_e .

Many theories have been proposed to explain how the contact angle changes with respect to parameters in the system (for details, see Berg 1993).

For θ_e close to 0, the apparent dynamic contact angle depends solely on the Capillary number Ca

$$Ca = \frac{\mu_L U}{\sigma_{LM}} \tag{1.2}$$

where μ_L is the viscosity of the liquid and U is the wetting speed,

$$\theta_a = f_H(\text{Ca}), \tag{1.3}$$

as first postulated by Hoffman (1975) using silicone oils in glass capillaries. Hoffman did not provide an explicit mathematical form for the universal master curve f_H he obtained. Tanner (1979), however, was the first one to derive the power law which is valid for $\text{Ca} \ll 1$,

$$\theta_a \approx \text{const} \cdot \text{Ca}^{1/3},$$
 (1.4)

from hydrodynamic theory, that fits Hoffman's experimental data. Voinov (1976), on the other hand, had obtained earlier a similar result from a hydrodynamic analysis. Thus, Eqn. 1.4 is referred to as the Hoffman-Voinov-Tanner (HVT) law (Kistler 1993). Numerous empirical correlations have also been proposed to include other dimensionless parameters or to capture the universal master curve obtained by Hoffman, such as Jiang's correlation (Jiang et al. 1979).

4 1. BASIC CONCEPTS

Cox (1986) provided a more general analysis of the dynamics of wetting. Cox's theory states that given two immiscible fluids with viscosity ratio $\lambda = \mu_M/\mu_L$ and at a leading order in Ca,

$$q(\theta_a) - q(\theta_e) = \operatorname{Ca}\ln(\epsilon^{-1}) \tag{1.5}$$

where θ_a is the apparent dynamic contact angle, θ_e is the static equilibrium contact angle, ϵ is a very small constant parameter, and the function $g(\theta)$ is given by

$$g(\theta) = \int_0^\theta \frac{d\Theta}{f(\Theta)} \tag{1.6}$$

and

$$f(\theta) = \frac{2\sin\theta\{\lambda^2(\theta^2 - \sin^2\theta) + 2\lambda[\theta(\pi - \theta) + \sin^2\theta] + [(\pi - \theta)^2 - \sin^2\theta]\}}{\lambda(\theta^2 - \sin^2\theta)[(\pi - \theta) + \sin\theta\cos\theta] + [(\pi - \theta)^2 - \sin^2\theta](\theta - \sin\theta\cos\theta)}.$$
 (1.7)

Similar to the HVT law, Cox's theory is valid for Ca $\ll 1$ and λ Ca $\ll 1$. Furthermore, for liquid/solid systems with complete wetting ($\theta_s = 0$) and negligible air viscosity, Cox's theory and similar equations proposed by Hocking & Rivers (1982) and Voinov (1976) corroborate the experimental finding of Hoffman (1975) that the apparent contact angle is primarily a function of Ca (Kistler 1993).

A wealth of information regarding wetting can be found in (Adamson 1990; de Gennes 1992; Berg 1993; de Gennes *et al.* 2004) and references therein. An early review and interesting experiments on moving contact lines are discussed in Dussan (1979) and Dussan & Davis (1974), respectively.

CHAPTER 2

Applications

The study of capillary phenomena has gained much attention recently. This increasing interest is motivated not only by fascination in naturally-occuring phenomena such as motion of drops, bubbles, and waves but also its importance in applied fields ranging from industrial and biomedical and pharmaceutical to microfluidic systems. We discuss a few examples of these coming from two disciplines, powder metallurgy (Upadhayaya 2000) and microfluidics (Squires & Quake 2005; Karniadakis et al. 2005; Tabeling 2005). In particular, we are interested in the study of liquid phase sintering (German 1985) and two-phase flows at the microscale.

2.1. Liquid phase sintering

Liquid phase sintering is a technological process that combines different metals to make products like ceramics, alloys, lamp filaments, dental fillings, insulators, carbides, bearings, turbines, blades, knives, and many more. Our improved and growing knowledge of materials properties such as hardness, toughness, and melting temperature, have aided us in creating new materials that exhibit some properties that we desire. Take for example a cemented tungsten carbide with cobalt additive (WC-Co) used for cutting and machining tools. They have excellent hardness and fracture toughness as a result of the combination of tungten carbide's hardness and cobalt's toughness. For a recent review of the general process of sintering, see Olevsky (1998).

Described in a simpler way, the tungsten carbide and cobalt powders, of typical fine-grained sizes of about 1-10 microns in diameter, are evenly mixed and machine pressed. The cobalt has lower melting temperature which is about 1300°C. The mixed material is heated until the cobalt softens. The cobalt then wets the solid grains and occupy the pores in the microstructure and due to surface tension forces exerted by liquid bridges pulling the solid particles together, the material rapidly rearranges and the cobalt can occupy more pores leading to a more compact structure. This is actually the most important stage in the process as it contributes the most in the overall densification of the compact (German 1985). The next stage called solution-reprecipitation is slower but higher densification is still expected due to mass diffusion that initiates the growth of a larger grain at the expense of a smaller grain. This is called coarsening or Ostwald ripening. The last stage is much slower and is dominated by processes common to solid state sintering which include grain growth, contact growth, grain coalescence, and pore elimination that all contribute to a more dense structure. Interestingly, people from ancient Mesopotamia had long practiced a similar process to make clay bricks

6 2. APPLICATIONS

for constructing their homes and buildings. The clay bricks were made of clay in its liquid phase mixed with straw, pressed, and were either baked or sun-dried.

Some important factors influence the densification of the compact microstructure such as the amount of liquid present, particle size, solubility of the solid in liquid, contact angle, dihedral angle (German 1985). Moreover, wettability is the most significant phenomenon in liquid phase sintering, as stressed out by German (1985) and in experiments carried out by Motta *et al.* (2004) and Taguchi *et al.* (2004).

Theoretical work on the densification during liquid phase sintering is presented in (Kingery 1959). A densification rate as a function of time, particle size, and temperature is proposed. An analysis of the capillary forces in liquid-phase sintering have been done by Heady & Cahn (1970). They derived an interparticle force between two spherical particles connected by a liquid bridge. The interparticle force had two major contributions, the surface tension forces, and the pressure difference caused by the surface curvature. On the other hand, Huppmann & Riegger (1975) used a circle approximation and rederived this interparticle force as a function of interparticle distance. They performed an experiment on tungsten spheres coated with copper in which analytical and experimental results were compared.

Svoboda et al. (1995) developed a quantitative model for liquid phase sintering. Their densification rate accounts for rearrangement, grain shape accommodation by contact flattening, and pore filling and grain coarsening in the final stages of sintering. Their model, however, does not account for wettability. In addition, cases where small rearrangement were only considered. A pore filling theory is developed by Lee & Kang (1997). In their theory both densification and grain growth are taken into account in the calculation of shrinkage in contrast to Kingery's theory that only takes densification into account. A computer simulation of particle rearrangement in the presence of liquid is presented in (Lee et al. 1999). The calculated capillary force between particles connected by a liquid bridge is a function of their distance with constants related to the elasticity. Anestiev & Froyen (1999) have also studied the rearrangement process due to capillary forces by calculating mean interparticle distances in time. They extended the analysis of Heady & Cahn (1970) to include friction force arising from the movement of the spherical particle through the liquid.

A quantitative model that describes the evolution of the microstructure during liquid phase sintering with dependencies on the phase diagram of the system, surface energies, and complete physicochemical properties of the materials involved, has not, to the author's knowledge, been reported yet in the literature. Notably, one of the motivations of the present thesis stemmed from this observation.

2.2. Microfluidics

Microfluidics is a rapidly developing field that deals with the study of fluid flows in artificial microsystems. Promising applications of microfluidics include *lab-on-a-chip* systems such as DNA testing in a small portable device that may contain

miniaturized devices such as micro-pumps, valves, mixers, separators, and reactors. Micromixers are essential in a *lab-on-a-chip* device. It is well known that in microchannels the flow is laminar and mixing is only based on molecular diffusion. Thus to attain rapid mixing, the mixer should be designed so as to create more intermaterial surface where diffusion between fluids takes place. Early successful implementations of passive mixers can be found in (Liu *et al.* 2000; Stroock *et al.* 2002). In (Stroock *et al.* 2002) for example, asymmetric grooves were built at the bottom of the channel to create transverse secondary flows. Other applications of microfluidics include microfilter systems that can be used to collect and identify chemical or biological entities from the environment; micropropulsions and nozzles that are essential for microspacecrafts (Karniadakis *et al.* 2005).

Some challenges in microfluidics include effective manipulation of drops or bubbles in microchannels, effective separation of microparticles in a fluid medium, and chaotic mixing.

The role of surface tension in the formation and/or manipulation of drops is important, and the study of which is rapidly increasing, partly due to the many fascinating effects that can be observed and its numerous possible applications in engineering and technology.

For example, the use of a t-junction to generate droplets has been demonstrated by Thorsen $et\ al.\ (2001)$. In their study, there were two competing stresses, viscous stress that extend and drag the column of liquid to be formed to droplets and surface tension that tries to minimize the interfacial area. Different pattern formations have been shown that are largely affected by the geometrical properties of the system.

When a drop is placed on a solid surface, it spreads and finds its equilibrium configuration, that is, with the given interfacial energies, the drop assumes an equilibrium contact angle with the surface (see Fig. 1.2). By actively modifying these interfacial energies, the drop moves and adjusts to another equilibrium contact angle. There are many ways to effectively manipulate drops such as thermowetting, optowetting, and electrowetting (Squires & Quake 2005). Since surface tension is temperature dependent, the application of thermal gradients on a droplet lying on a horizontal surface induces a gradient in surface tension, which in turn induces a Marangoni flow in the droplet that makes it able to move (Brochard 1989). The concept has been successfully applied in DNA analysis devices (Burns et al. 1998).

The use of light can also drive a droplet into motion. Ichimura *et al.* (2000) demonstrated the manipulation of drops reversibly by spatially controlled photoir-radiation of a photosensitive substrate surface.

By the application of a potential difference between the drop and the substrate, the solid/liquid surface behaves as a capacitor and its interfacial tension σ_{SL} decreases. With the modified interfacial tension, the drop adjusts to a new equilibrium contact angle given by the Lippman equation (Squires & Quake 2005).

In this thesis the study of free surface flows at the microscale is presented. The aim has been to model and simulate different phenomena involving flows mainly

8 2. APPLICATIONS

driven by capillarity. The emphasis is on the importance of surface and geometrical properties of a given system, and how surface tension plays a significant role.

CHAPTER 3

Mathematical modeling

3.1. Modeling wetting

The wetting phenomena can be viewed as a free interface problem where the interface between the two immiscible fluids are deformable and free to change their shape in order to minimize their surface energy. The problem can be modeled with the front-tracking (Unverdi & Tryggvason 1992), level set (Sussman et al. 1994), volume-of-fluid (Hirt & Nichols 1981), or diffuse-interface methods such as the phase-field method (Jacqmin 1999). Interestingly, molecular dynamics simulations has also been used to study the dynamics of wetting (Yang et al. 1991; Coninck et al. 1995; Fan & Cagin 1995; Jin et al. 1997).

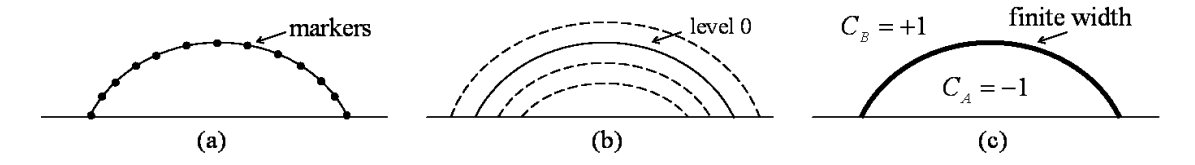


FIGURE 3.1. Modeling wetting with (a) front-tracking, (b) level set, and (c) phase-field method.

The front-tracking method explicitly tracks an interface by markers, see Fig. 3.1a. The Lagrangian markers are evenly distributed on the interface together with some connectivity. The markers are advected by a velocity field defined on a discrete Eulerian grid by which interpolation of the velocity field from the grid to the Lagrangian points is implemented. In many cases, clustering occurs, so markers are inserted or deleted to preserve the quality of the interface. In 3D with surface elements, this gets much more complicated.

In the standard level set method, a signed distance function φ is used. The interface is defined as having the zero contour (see Fig. 3.1b). The movement of the interface is governed by a partial differential equation of Hamilton-Jacobi type, i.e., $\partial_t \varphi + \mathbf{u} \cdot \nabla \varphi = 0$. Similar to the front-tracking, clustering of contours takes place, so reinitialization is done to preserve the property of the signed distance function. An issue of non-conservation of this method has been addressed, for example, in (Olsson & Kreiss 2005). An application of the level set method to moving contact lines has been presented, for example, in (Singh & Joseph 2005; Mukherjee & Kandlikar 2007; Lesage et al. 2007; Son & Hur 2007). The contact angle is prescribed on the solid surface with $\mathbf{n} \cdot (\nabla \varphi / |\nabla \varphi|) = \cos \theta$, where \mathbf{n} is the unit outer normal on the solid surface and θ is the contact angle. The contact line

will move according to a slip velocity, taken either by relaxing the no-slip boundary condition in which the slip velocity is proportional to the shear stress on the wall, or compute an 'effective numerical slip' in terms of the prescribed contact angle, (for details, see Singh & Joseph 2005).

The level set has been coupled to the volume-of-fluid method to combine their advantages, a more accurate interfacial curvature of the level set and the conservation properties of the volume-of-fluid (Son & Hur 2002). In the volume-of-fluid method, a color function ζ is introduced to identify the shape and evolution of the interface. The function distinguishes one fluid from another by associating a distinct value for each bulk phases, say 0 and 1. Computational cells that have values between 0 and 1 are assumed to contain part of the interface. Similar to the level set, the movement of the interface is governed by $\partial_t \zeta + \mathbf{u} \cdot \nabla \zeta = 0$. An inherent difficulty in this method is the reconstruction of the interface by finding an approximation to the section of the interface in each computational cell given only the volume/area fraction ζ .

In this thesis, diffuse-interface methods are implemented. Some advantages of such models are mass conservation, handles topological changes very well, no intervention required during simulation, and flexibility to simulate 2D, axisymmetric, and 3D flows.

3.2. Diffuse-interface methods

Diffuse-interface methods consider the interface between the two fluids to have a non-zero thickness endowed with physical properties such as surface tension. For a review of the development of diffuse-interface models applied to different interfacial phenomena, see Anderson et al. (1998). Phase-field models are particular type of diffuse-interface models that are based on fluid free energy, an idea that can be traced to van der Waals (1893). For reviews of phase-field models and simulations for microstructure evolution, see (Chen 2002; Boettinger et al. 2002). The main drawback of phase-field models is the thickness of the interface. Although in reality there is an existing region where a property of one fluid changes to the other, the current capability of computers only allows us to have a thickness way much more than the thickness of this region.

Two commonly employed phase-field models are the Cahn-Allen and Cahn-Hilliard theory. Cahn-Allen equations describe the evolution of a nonconserved quantity and commonly used in solidification and nucleation problems (Boettinger et al. 2002; Loginova et al. 2003, among many others). The Cahn-Hilliard theory, on the other hand, describe the evolution of a conserved order parameter and is used in spinodal decomposition problems (see for example Cahn 1961; Badalassi et al. 2003; Kim et al. 2004), contact-line dynamics (Seppecher 1996; Jacqmin 1999, 2000; Villanueva & Amberg 2006, to name a few), microfluidics applications (Villanueva et al. 2007, or Paper 2 in this thesis), and many more.

One notable feature of the Cahn-Hilliard theory is that the force singularity arising in the classical model of moving contact lines as pointed out by Huh & Scriven (1971) is no longer present due to mass transfer across the interface, for details see Seppecher (1996). Whereas other methods require some special treatment on the contact line region to make it move.

In what follows is a derivation of the Cahn-Hilliard equation based on the works of (van der Waals 1893; Cahn 1961; Jacqmin 1999).

Consider the case of an isothermal, viscous, incompressible binary fluid consisting of two components, A and B. We can introduce an order parameter, a phase-field C, to characterize the two different phases which is analogous to the relative concentration between the two. In each bulk phase, C assumes a distinct constant value and changes rapidly but smoothly in the interfacial region. For example, component A assumes the value $C_A = -1$ while component B takes the value $C_B = 1$ and the transition from C_A to C_B describes the interfacial region (see Fig. 3.1c).

The free energy of the system can be postulated as

$$\mathcal{F} = \int_{\Omega} (\beta \Psi(C) + \frac{1}{2} \alpha (\nabla C)^2) d\Omega + \int_{\partial \Omega} [\sigma_{SL} + (\sigma_{SM} - \sigma_{SL}) g(C)] dS$$
 (3.1)

that is the sum of the bulk energy $\beta\Psi(C)$, gradient energy $\frac{1}{2}\alpha(\nabla C)^2$, and wall free energy $\sigma_{SL} + (\sigma_{SM} - \sigma_{SL})g(C)$. The function Ψ is a double-well positive function that has two minima corresponding to the two stable phases. A simple example of such function is $(C+1)^2(C-1)^2$ which has minima at $C_{A,B} = \pm 1$ and a peak of high energy at C=0. The constant parameters α and β are used to control the surface tension and the interface thickness. The function g(C) is chosen such that $g(C_A) = 0$ and $g(C_B) = 1$. The parameter σ_{SL} is the interfacial energy between the solid and the liquid and σ_{SM} is the interfacial energy between the solid and the medium.

Consider a variation in \mathcal{F} ,

$$\delta \mathcal{F} = \int_{\Omega} \left\{ \beta \Psi'(C) \delta C + \alpha \nabla C \delta(\nabla C) \right\} d\Omega + \int_{\partial \Omega} (\sigma_{SM} - \sigma_{SL}) g'(C) \delta C dS \quad (3.2)$$

then integration by parts yields,

$$\delta \mathcal{F} = \int_{\Omega} \left\{ \beta \Psi'(C) - \alpha \nabla^2 C \right\} \delta C \, d\Omega$$

$$+ \int_{\partial \Omega} \left\{ \alpha \mathbf{n} \cdot \nabla C + (\sigma_{SM} - \sigma_{SL}) g'(C) \right\} \delta C \, dS.$$
(3.3)

The boundary integral vanishes by taking,

$$\alpha \mathbf{n} \cdot \nabla C + (\sigma_{SM} - \sigma_{SL})g'(C) = 0, \quad \text{on } \partial\Omega,$$
 (3.4)

which is called the wetting condition. Define the chemical potential η

$$\eta = \beta \Psi'(C) - \alpha \nabla^2 C. \tag{3.5}$$

The variation in \mathcal{F} is simplified to,

$$\delta \mathcal{F} = \int_{\Omega} \eta \delta C \, d\Omega. \tag{3.6}$$

12 3. MATHEMATICAL MODELING

Any variation in composition δC causes a variation in free energy $\delta \mathcal{F}$, however, it is not known at this point if the free energy \mathcal{F} increases or decreases as a result. Looking at it in a different way, if we postulate that the free energy of the system must always decrease, obeying laws of thermodynamics, then we should only allow certain variations in composition that satisfy our assumption.

Note that the composition obeys mass conservation,

$$\frac{\partial C}{\partial t} + \nabla \cdot J = 0 \tag{3.7}$$

where J is a flux.

Now, consider a variation in C,

$$\delta C = \frac{\partial C}{\partial t} dt = -dt \nabla \cdot J \tag{3.8}$$

where dt is an infinitesimal time. Substitution of Eqn. 3.8 into Eqn. 3.6 and using the divergence theorem give

$$\delta \mathcal{F} = -dt \int_{\Omega} \eta \nabla \cdot J \, d\Omega$$

$$= dt \int_{\Omega} J \cdot \nabla \eta \, d\Omega - \int_{\partial \Omega} (\mathbf{n} \cdot J) \eta \, dS.$$
(3.9)

The boundary integral vanishes by taking,

$$\mathbf{n} \cdot J = 0 \qquad \text{on } \partial\Omega. \tag{3.10}$$

which means no flux is allowed across the boundary.

Simply,

$$\delta \mathcal{F} = dt \int_{\Omega} J \cdot \nabla \eta \, d\Omega. \tag{3.11}$$

Our aim is to guarantee a decrease in free energy after an infinitesimal time dt, that is, the evolution of C is such that $\delta \mathcal{F} < 0$. Choosing the flux to be of the form

$$J = -\kappa \nabla \eta, \qquad \kappa > 0 \tag{3.12}$$

and substitution into Eqn 3.11, we have

$$\delta \mathcal{F} = -dt \int_{\Omega} \kappa \nabla \eta \cdot \nabla \eta \, d\Omega = -dt \int_{\Omega} \kappa (\nabla \eta)^2 \, d\Omega < 0, \tag{3.13}$$

which guarantees a decrease in free energy.

Thus, the Cahn-Hilliard equation, modified to account for fluid motion, is given by

$$\frac{\partial C}{\partial t} + (\mathbf{u} \cdot \nabla)C = \kappa \nabla^2 \eta \qquad \text{in } \Omega \times T$$

$$\eta = \beta \Psi'(C) - \alpha \nabla^2 C \qquad \text{in } \Omega \times T$$

$$\mathbf{n} \cdot \nabla \eta = 0 \qquad \text{on } \partial \Omega$$

$$\alpha \mathbf{n} \cdot \nabla C + (\sigma_{SM} - \sigma_{SL})g'(C) = 0 \qquad \text{on } \partial \Omega$$

$$C(\cdot, 0) = C_0 \qquad \text{in } \Omega$$
(3.14)

where $\mathbf{u}(\mathbf{x},t)$ is the velocity field and κ assumed to be constant. The Cahn-Hilliard equation models the creation, evolution, and dissolution of diffusively controlled phase-field interfaces (Bates & Fife 1993).

3.3. Navier-Stokes flow

The isothermal, viscous, and incompressible Navier-Stokes equations form the basis for studying many phenomena concerning fluid flow. The system consists of partial differential equations expressing conservation of momentum and mass, respectively, and reads

$$\rho \left(\frac{\partial \mathbf{u}}{\partial t} + \mathbf{u} \cdot \nabla \mathbf{u} \right) = -\nabla p + \nabla \cdot \left(\mu (\nabla \mathbf{u} + \nabla \mathbf{u}^T) \right) + F \quad \text{in} \quad \Omega \times T$$

$$\nabla \cdot \mathbf{u} = 0 \quad \text{in} \quad \Omega \times T$$

$$\mathbf{u}(\cdot, 0) = \mathbf{u}_0 \quad \text{in} \quad \Omega$$
(3.15)

where ρ is the density, μ is the viscosity, $\mathbf{u}(\mathbf{x},t)$ is the velocity vector, $p(\mathbf{x},t)$ is the pressure, and F is the sum of all the given driving forces such as surface tension and gravity forces.

A surface tension force that is related to the order parameter is needed when coupling the Navier-Stokes equations with the Cahn-Hilliard equation. Following the derivation of Jacqmin (1999), the free energy changes in time due to convection according to:

$$\frac{\partial \mathcal{F}}{\partial t}\Big|_{t=0} = \int_{\Omega} \frac{\delta \mathcal{F}}{\delta C} \frac{\partial C}{\partial t}\Big|_{t=0} d\Omega$$
 (3.16)

Note that

$$\left. \frac{\partial C}{\partial t} \right|_{\text{conv}} = -\nabla \cdot (\mathbf{u} \, C).$$
 (3.17)

Integration by parts combined with the divergence theorem yield,

$$\frac{\partial \mathcal{F}}{\partial t} \Big|_{\text{conv}} = -\int_{\Omega} \frac{\delta \mathcal{F}}{\delta C} \nabla \cdot (\mathbf{u} C) d\Omega,
= -\int_{\partial \Omega} \mathbf{n} \cdot \left(\frac{\delta \mathcal{F}}{\delta C} \mathbf{u} C \right) dS + \int_{\Omega} \mathbf{u} \cdot C \nabla \left(\frac{\delta \mathcal{F}}{\delta C} \right) d\Omega.$$
(3.18)

14 3. MATHEMATICAL MODELING

The boundary integral vanishes due to boundary conditions. The rate of change of kinetic energy E due to surface tension forcing is always opposite to the change in free energy. Then,

$$-\frac{\partial \mathcal{F}}{\partial t}\Big|_{\text{conv}} = \frac{\partial E}{\partial t}\Big|_{\text{kinetic}} = \int_{\Omega} \mathbf{u} \cdot F \, d\Omega. \tag{3.19}$$

Thus the surface tension forcing is given by

$$F = -C\nabla\left(\frac{\delta\mathcal{F}}{\delta C}\right) = -C\nabla\eta. \tag{3.20}$$

It is demonstrated in (Anderson *et al.* 1998) that diffuse-interface models such as the one presented here approach asymptotically the free-boundary formulation which is done by adopting the sharp-interface limit.

CHAPTER 4

Computational aspects

4.1. Numerical treatment

Partial differential equations (PDEs) are mathematical descriptions of many physical phenomena. Their exact or classical solutions cannot be found in most cases. In the era of scientific computing, many numerical methods have been proposed to find an approximate solution of the original PDE. Common methods include the finite difference, spectral, finite volume, and finite element method.

In the finite difference method, the domain is discretised with a finite number of grid points. Approximate solution at the grid points is obtained by replacing derivatives with an appropriate difference quotients (stencils). The finite difference method, owing to its simplicity and ease of use, has been used in many phase-field calculations (Wheeler et al. 1993; Warren & Boettinger 1994; Murray et al. 1995; Braun et al. 1997).

Spectral methods assume wavelike solutions of the underlying PDE. They have advantages in solving periodic problems, among others and have also been successfully applied in the study of hydrodynamic stabities in shear flows (Schmid & Henningson 2001).

Finite volume methods are also commonly used especially in commercial Computational Fluid Dynamics (CFD) codes. Here, the domain is discretised into control volumes and then nodal/vertex values that are typically located at the center of the control volume are sought by solving the governing equations integrated over the control volume.

In this thesis, the finite element method is used. The finite element method is known to be a powerful and flexible tool for flows with complicated geometries.

4.2. Finite element discretisation

The Galerkin finite element method finds weak solutions of a variational/weak form by a piecewise polynomial approximation in space, time, or space/time. The finite element method is very popular in the structural mechanics community where it originated and it is recently gaining popularity in solving fluid dynamical problems especially in flows with complicated geometries, (for a thorough numerical treatment of the subject, refer to Gresho & Sani 1998).

The standard procedure for setting up the variational form is to multiply the PDE with a test function and integrate over the entire domain. Apply integration by parts where necessary and choose appropriate function spaces.

As an example, the variational formulation of the Cahn-Hilliard equation (Eqn. 3.14) without convection for simplicity, reads: Find $C, \phi \in \mathcal{H}^1(\Omega)$ such that for almost all $t \in (0,T)$

$$(\frac{\partial C}{\partial t}, \chi) + \kappa(\nabla \phi, \nabla \chi) = 0 \qquad \forall \chi \in \mathcal{H}^{1}(\Omega)$$

$$(\phi, \chi) - \beta(\Psi'(C), \chi) - \alpha(\nabla C, \nabla \chi) - \gamma(g'(C), \chi)_{\Gamma} = 0 \quad \forall \chi \in \mathcal{H}^{1}(\Omega)$$

$$(4.1)$$

where (\cdot, \cdot) is the L^2 -scalar product and $\gamma = \sigma_{SM} - \sigma_{SL}$. An L_2 -space is defined as $L_2(\Omega) = \{v | \int_{\Omega} v^2 < \infty\}$ while the Hilbert space $H^1(\Omega) = \{v | v \in L_2(\Omega), \nabla v \in U \in L_2(\Omega)\}$ $L_2(\Omega)$.

We now proceed in setting up a Galerkin finite element discretisation of the coupled Cahn-Hilliard and Navier-Stokes equations. We simplify the discussion by assuming a homogeneous Dirichlet boundary condition for the velocity, and specific use of continuous piecewise linear functions. Our finite element treatment for the Navier-Stokes is similar to those of Hansbo & Szepessy (1990) without the streamline diffusion method.

Let $\mathcal{F} = \{\tau\}$ be a finite element triangulation of $\bar{\Omega}$ where the elements τ have the smallest angle uniformly bounded away from 0. Let $0 = t_0 < t_1 < \cdots < t_N = T$ be a partition of [0,T] into subintervals $I_n=(t_n,t_{n+1})$ of lengths $k_n=t_{n+1}-t_n$ and introduce space-time 'slabs' $S_n=\Omega\times I_n$. For $n=0,1,\ldots,N$, let $K_h^n=\{\eta\}$ be the corresponding subdivision of S_n into elements $\eta=\tau\times I_n$ and define

$$V_{h}^{n} = \{ v \in [\mathcal{H}^{1}(S_{n})]^{d} : v|_{\eta} \in P_{1}(\tau) \times P_{1}(I_{n}) \,\forall \eta = \tau \times I_{n} \in K_{h}^{n}, v = 0 \text{ on } \Gamma \times I_{n} \}$$

$$V_{h} = \prod_{n=0}^{N} V_{h}^{n}$$

$$Q_{h}^{n} = \{ q \in \mathcal{H}^{1}(S_{n})|q|_{\eta} \in P_{1}(\tau) \times P_{1}(I_{n}) \,\forall \eta = \tau \times I_{n} \in K_{h}^{n} \}$$

$$Q_{h} = \prod_{n=0}^{N} Q_{h}^{n}$$

$$(4.2)$$

where $P_1(\omega)$ denotes the set of polynomials of degree one on ω and d=1,2,3 is the space dimension.

The finite element approximation now reads: Find $(C, \phi, \mathbf{u}, p) \in Q_h \times Q_h \times V_h \times V_h$ Q_h such that for $n = 0, 1, \dots, N$,

$$\left(\frac{\partial C}{\partial t} + \mathbf{u} \cdot \nabla C, q\right)_{S_n} + \kappa(\nabla \phi, \nabla q)_{S_n} = 0, \tag{4.3a}$$

$$(\phi, q) - \beta(\Psi'(C), q)_{S_n} - \alpha(\nabla C, \nabla q)_{S_n} - \gamma(g'(C), q)_{\Gamma \times I_n} = 0, \tag{4.3b}$$

$$(\rho \frac{\partial \mathbf{u}}{\partial t} + \rho \mathbf{u} \cdot \nabla \mathbf{u} + \nabla p, \mathbf{v})_{S_n} + \mu (\nabla \mathbf{u}, \nabla \mathbf{v})_{S_n} = (F, \mathbf{v})_{S_n},$$

$$(\nabla \cdot \mathbf{u}, q)_{S_n} = 0, \qquad \forall (\mathbf{v}, q) \in V_h^n \times Q_h^n$$

$$(4.3d)$$

$$(\nabla \cdot \mathbf{u}, q)_{S_n} = 0, \qquad \forall (\mathbf{v}, q) \in V_h^n \times Q_h^n$$
 (4.3d)

where $(\cdot, \cdot)_{\Lambda}$ is the L_2 -scalar product in $L_2(\Lambda)$.

Solving the Navier-Stokes equations implicitly is computationally expensive. This is one reason why the use of projection methods are increasingly popular (Gresho & Sani 1998; Guermond et al. 2006). In projection methods, one needs to solve at each time step a sequence of decoupled equations for the velocity and pressure. As an example, we present the incremental fractional-step algorithm presented in (Guermond & Quartapelle 1998). In this scheme, the pressure at the viscous step is made explicit and then corrected at the projection step. The scheme is presented using the original form of the Navier-Stokes.

The first step is to consider an advection-diffusion equation

$$\rho \frac{\mathbf{u}^{n+1} - \hat{\mathbf{u}}^n}{k_{n+1}} + \rho \mathbf{u}^n \cdot \nabla \mathbf{u}^{n+1} - \mu \nabla^2 \mathbf{u}^{n+1} + \nabla p^n = F^{n+1}$$

$$(4.4)$$

then perform the projection step

$$\rho \frac{\hat{\mathbf{u}}^{n+1} - \mathbf{u}^{n+1}}{k_{n+1}} + \nabla (p^{n+1} - p^n) = 0, \tag{4.5a}$$

$$\nabla \cdot \hat{\mathbf{u}}^{n+1} = 0. \tag{4.5b}$$

Applying $\nabla \cdot$ in Eqn.4.5a, a Poisson equation for the pressure is obtained,

$$-\nabla^{2}(p^{n+1} - p^{n}) = -\frac{\rho}{k_{n+1}} \nabla \cdot \mathbf{u}^{n+1}.$$
 (4.6)

With the relation $\hat{\mathbf{u}}^n = \mathbf{u}^n - \frac{k_{n+1}}{\rho} \nabla (p^n - p^{n-1})$, the end-of-step velocity can be eliminated and the viscous step becomes

$$\rho \frac{\mathbf{u}^{n+1} - \mathbf{u}^n}{k_{n+1}} + \rho \mathbf{u}^n \cdot \nabla \mathbf{u}^{n+1} - \mu \nabla^2 \mathbf{u}^{n+1} + \nabla (2p^n - p^{n-1}) = F^{n+1}. \tag{4.7}$$

The finite element discretisation of the two Equations 4.7 and 4.6 can be done in a similar way as discussed above.

Furthermore, a pressure stabilization term $\epsilon_h(\nabla p, \nabla q)_{s_n}$ where $\epsilon \sim h^2$ can be added in the projection step to improve stability. The pressure stabilization term with the above equal-oder interpolation circumvents the Ladyshenskaya-Babuska-Brezzi (LBB) condition (Hughes *et al.* 1986).

More detailed discussions on the finite element analysis of the Cahn-Hilliard equation can be seen in (Elliott & Larsson 1992; Barrett & Blowey 1995, 1999; Garcke et al. 2001; Barrett & Blowey 2002) and references therein. While finite element analysis of the Navier-Stokes equations including streamline diffusion methods, adaptive methods, projection methods, etc., can be found in (Hansbo & Szepessy 1990; Hoffman 2002; Becker & Rannacher 2001; Gresho & Sani 1998). For a general numerical treatment of PDEs, refer to (Eriksson et al. 1996; Larsson & Thomée 2003) along with (Debnath & Mikusinski 1999; Evans 1998).

After setting up the finite dimensional analog of the weak form, the next step is to solve the corresponding discrete system of equations.

Using the basis of hat functions $\{\Phi_j\}_{j=1}^M$, we have for example for the variable C,

$$C(\mathbf{x},t) = \sum_{j=1}^{M} \psi_j(t)\Phi_j(\mathbf{x})$$
(4.8)

and determine the nodal values ψ_j at time t using the Galerkin orthogonality (Eqn. 4.3a). The hat function Φ_j associated to node \mathbf{x}_j has the property that $\Phi_j \in Q_h$ and $\Phi_j(\mathbf{x}_l) = 1$ if j = l and $\Phi_j(\mathbf{x}_l) = 0$ otherwise. Substitution of Eqn. 4.8 into Eqn. 4.3a leads to a $M \times M$ linear system of equations,

$$A\psi = b \tag{4.9}$$

where b is the load vector that comes from both the previous solution and the second term of Eqn. 4.3a if that is taken explicitly.

A finite linear system of algebraic equations can be solved in two ways, direct methods or iterative methods. For dense matrices (with few zeros), it is advantageous to use direct methods. While for sparse matrices, iterative methods are generally used such as the generalized minimum residual method (GMRES), conjugate gradient method (CG), multigrid method, etc. (for further reading, see Saad 1996). While the GMRES is more oftenly used, the CG method performs very well with symmetric and positive definite matrices. The use of preconditioners is also essential for a more efficient algorithm. It should also be noted that there is no definite general guidelines on which iterative method to use.

Different numerical schemes have been proposed to treat the Cahn-Hilliard/Navier-Stokes system (Badalassi *et al.* 2003; Kim *et al.* 2004). Here a simple numerical scheme is proposed and described as follows: At every time step,

- 1. Advect the composition C with $C_t + \mathbf{u} \cdot \nabla C = 0$. The streamline diffusion method can be included in this step.
- 2. Linearize and lump the chemical potential η . While solving for the non-convective C with a CG, η is updated and solved inside CG's iteration loop. A diagonal solve is used to compute η in this step.
- 3. Solve η again with a standard CG for a more accurate surface tension forcing in the Navier-Stokes equations.
- 4. Solve the Navier-Stokes equations using a projection method. A pressure stabilization term can be included.

This scheme has been successfully applied in (Villanueva et al. 2007, or Paper 2 in this thesis) under the framework of a finite element solver called FemLego (Amberg et al. 1999; Do-Quang et al. 2007).

The computational error using the finite element method has three sources: (1) Galerkin discretization, because the solution is approximated by piecewise polynomials, (2) numerical quadrature error arising from evaluating the integrals, (3) solution of the discrete problem, from solving the resulting discrete systems only approximately. For more details, see (Eriksson *et al.* 1995).

4.3. Parallel adaptive computation

In most initial value problems the regions of interest occur only in certain parts of the domain. Mesh adaptivity offers a way to greatly reduced the computational cost of solving the initial value problem given a computational resources and a desired accuracy. In this way, computational resources are more concentrated on regions where the solution changes rapidly. The use of mesh adaptive computations are almost mandatory in many problems especially in convection-dominated problems and free boundary flows. In many cases both mesh refinement and derefinement are needed. While refinement tries to keep the solution accurate enough, derefinement makes the computation as efficient as possible by making sure that computational resources are not wasted or unnecessarily used. For the same reason of reducing the computational and storage requirements, the adaptive computation can be done in a parallel computing environment.

Some transient problems are way too complex to be solved without the use of parallel adaptivity. However, the design and implementation of an efficient and reliable parallel adaptive algorithm remains difficult because there are many issues that must be resolved especially in the parallel implementation.

For a parallel solver to be efficient, the total workload must be evenly distributed to each processor which is done by partitioning the mesh in such a way that each processor takes the same number of elements and communication between processors should be kept minimum. The communication between processors and exchange of data can also be made efficient by having a sound data management (Laszloffy et al. 2000) as well as keeping less information to be shared with other processors. Since computational power of individual processors can be increased with increasing demand, focusing more on ways of improving communication between processors offers a great deal of efficiency. Without adaptivity, the mesh does not change and exchange of information is limited only on the data on the partition boundary. Mesh repartitioning is also unnecessary as well as mesh migration. The inclusion of adaptivity, however, which is done in parallel often requires the mesh to be repartitioned to keep a balanced workload. Mesh migration is then unavoidable. Moreover, the standard use of adaptive refinement/derefinement also requires keeping the history of refinements, to facilitate derefinement and maintain the nestedness of the mesh (Rivara 1989). But this greatly increases the communication cost because it is an added information that has to be shared between processors and also requires some memory to keep the information. A scheme proposed by (Do-Quang et al. 2007, or Paper 3 in this thesis), however, does not keep the history of refinement but keeps a local information about the node and edge level. This information can be used to track back to the previous level of mesh refinement, i.e., it is used to identify which nodes, edges or faces to be removed and generate another set of information to be used for the next level of derefinement.

CHAPTER 5

Summary of results

Paper 1. Some generic capillary-driven flows.

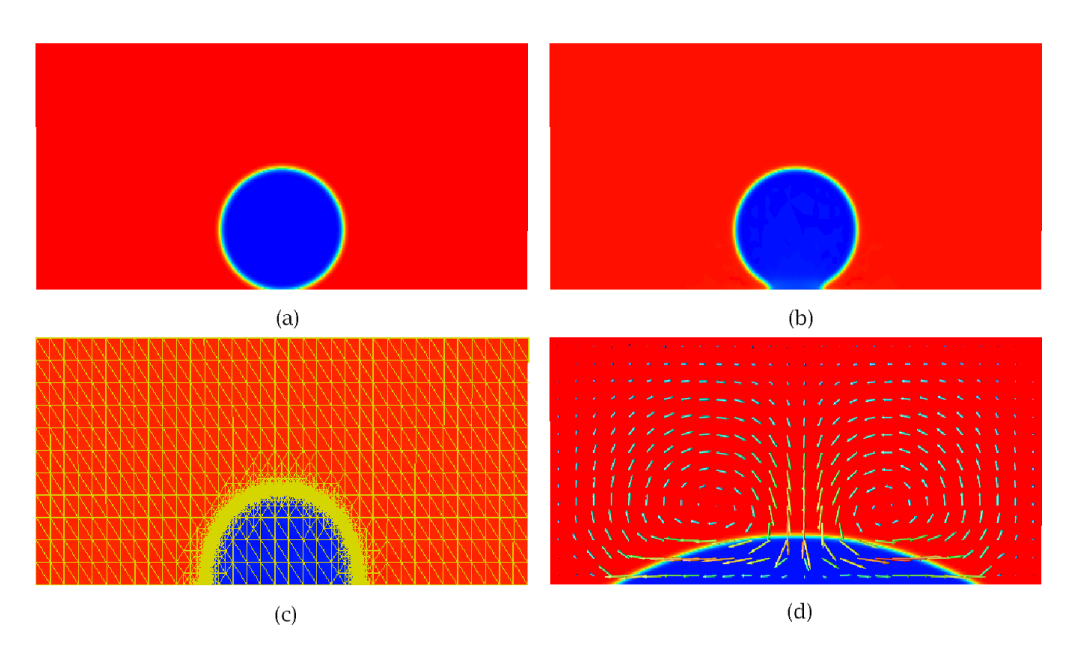


FIGURE 5.1. Wetting of a liquid droplet on a solid surface. Concentration field at nondimensional time t=0,1,10,200 with Ca = 1.0, Re = 1.0, Pe = $1.5 \cdot 10^4$, Cn = 0.01 and k=0.9063 ($\theta_e \approx 25^\circ$). The mesh and velocity field are superimposed in (c) and (d), respectively.

In this paper, numerical simulations of some generic capillary-driven flows such as basic wetting of a liquid drop on a solid surface, sintering-like flows, and imbibition of of liquids into a porous medium are presented. The coupled Cahn-Hilliard/Navier-Stokes system previously discussed is nondimensionalized and used to model the given problems.

Figure 5.1a shows a 2D drop lying on a solid surface with Ca = 1.0, Re = 1.0, Pe = 10^4 , and Cn = 0.01. The wetting coefficient is k = 0.9063 which is equivalent to $\theta_e \approx 25^\circ$ using Eqn. 1.1. The drop is surrounded by another liquid with density and viscosity similar to the drop. In Fig. 5.1a, the drop is in contact with the surface at 158° apparent contact angle. Then the drop starts to spread and wets the surface with a 141° apparent contact angle (Fig. 5.1b). In Fig. 5.1c,

the drop spreads further with 77° apparent contact angle. The adaptive mesh is superimposed and shows fine resolution along the vicinity of the interface. Finally, the drop closely reaches the equilibrium contact angle of $\theta_e \approx 25^{\circ}$ in Fig. 5.1d. The spreading is fast in the first stage and then slowly reach the equilibrium static contact angle. The velocity field is also superimposed and gives a symmetric profile with two vortices. In the final time considered, we measured an apparent contact angle of 26°, one degree higher than the theoretically set value of 25°.

The apparent contact angle is also plotted versus the Capillary number for different interface thicknesses in Figure 5.2. The limited scatter that is present in Fig. 5.2 is attributed to uncertainites in determining the apparent contact angle. Nevertheless, the apparent contact angle is found to be fairly independent of the interface thickness. Moreover, the values taken on the dependence of the contact angle on the Capillary number is fairly close to Cox's theory (see Section 1) with viscosity ratio $\lambda=1$, parameter $\epsilon=0.05$, and static equilibrium contact angle $\theta_e=25^{\circ}$. This result is an update of Paper 1. The numerical results were compared with Cox's theory as opposed to Hoffman's experiment that was shown in the appended paper. The values of Hoffman's experiment were for silicone oils in air.

Paper 2. Microdroplet deposition under a liquid medium.

It this paper, a numerical and experimental study of the factors affecting reproducibility of depositing microdroplets under a liquid medium is presented. In the deposition procedure, sample solution is dispensed from the end of a capillary by means of a pressure pulse onto a substrate with pillar-shaped sample anchors. The model used is the Cahn-Hilliard/Navier-Stokes sytem, similar to the one used in Paper 1 except that gravity forces are included. We have implemented a semi-implicit scheme to avoid a severe time-step restriction imposed by the fourth order Cahn-Hilliard equation. An axisymmetric model with mesh adaptivity was implemented. The results showed that the deposited volume mainly depends on the capillary-substrate distance and the anchor surface wettability. A critical equilibrium contact angle has been identified below which reproducible depositions are facilitated.

Figure 5.3 shows an experimental microdroplet deposition of acetonitrile/water made from a height of $96\mu m$ under liquid fluorocarbon on a $50\mu m$ anchor. The corresponding numerical microdroplet deposition made from a height of $100\mu m$ is shown in Fig. 5.4. The numerical simulations capture the deformation of the liquid column and the pinning of the wetting lines on the edges of both surfaces. The volume of the deposited droplet in the simulation is 28 pL compared to the experimental value of 27 ± 1 pL.

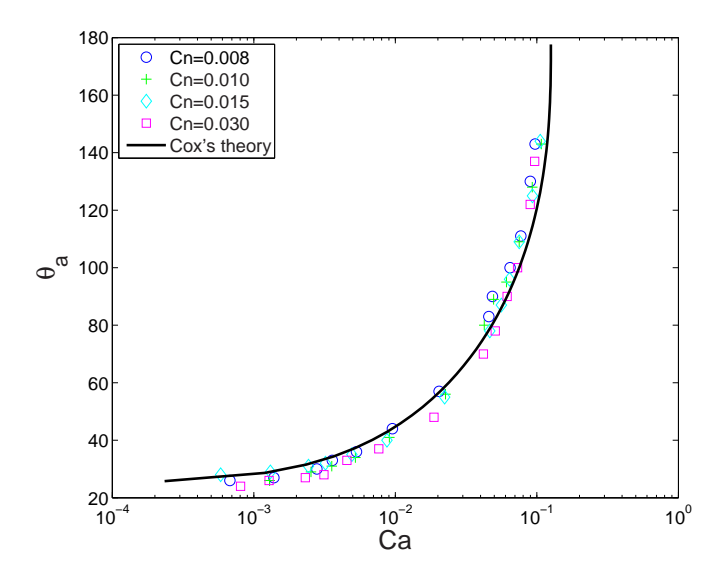


FIGURE 5.2. Dependence of the contact angle on the Capillary number: (\circ), (+), (\diamond), and (\square) with different Cahn number Cn and (-) Cox's theory with viscosity ratio $\lambda = 1$, $\epsilon = 0.05$, and $\theta_e = 25^{\circ}$ (see Eqn. 1.5).

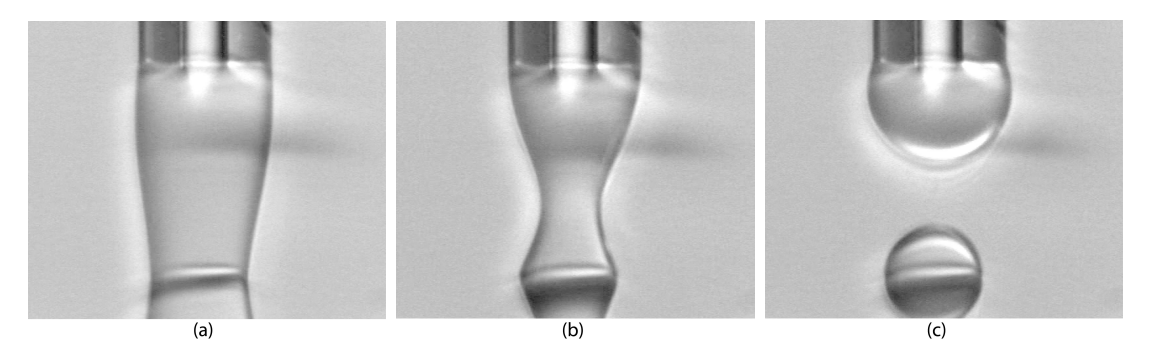


FIGURE 5.3. Experimental microdroplet deposition of acetonitrile/water made from a height of $96\mu m$ under liquid fluorocarbon on a $50\mu m$ anchor. The volume deposited is 27 ± 1 pL.

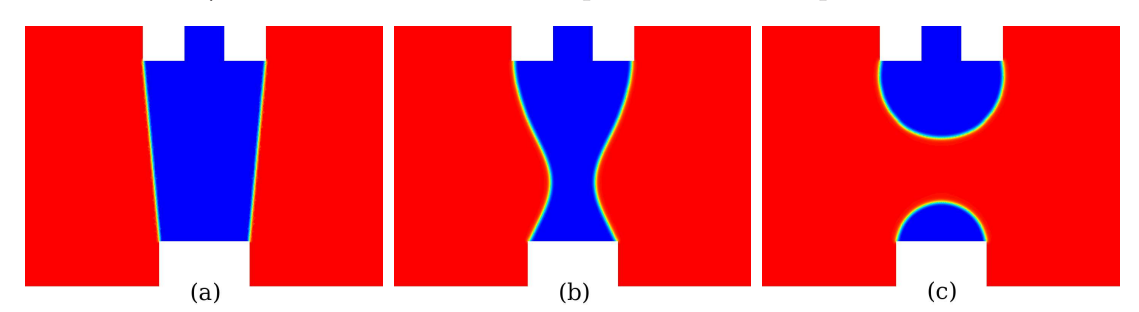


FIGURE 5.4. Numerical microdroplet deposition made from a height of $100\mu m$. The volume deposited is 28 pL.

Paper 3. Parallel adaptive computation of some time-dependent materials-related microstructural problems.

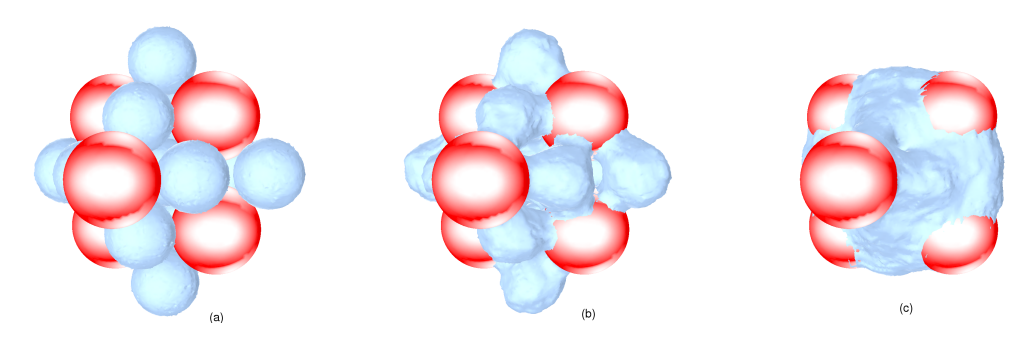


FIGURE 5.5. Three-dimensional generic sintering with a fixed matrix of solid particles (larger spheres). Isosurface at t = 0, 2, 10 with Ca = 0.1, Re = 0.1, and $Pe = 10^4$.

In this paper, some materials-related microstructural problems calculated using the phase-field method are presented. A proposed parallel adative scheme is used to perform the calculations. The scheme keeps the level of node and edge for 2D and level of node and face for 3D instead of the complete history of refinements to facilitate derefinement. The information is local and exchange of information is minimized and also less memory is used. The parallel adaptive algorithms that run on distributed memory machines are implemented in the numerical simulation of dendritic growth and capillary-driven flows.

In Fig. 5.5, a successful implementation of the scheme to simulate capillary-driven flows is demonstrated. The compact microstructure consists of six solid particles (larger spheres) and thirteen softer drops that are evenly distributed. The drops spread over the solid grains and phase deformation, coalescence, pore migration and pore elimination take place. The numerical simulations also demonstrate the flexibility of the Cahn-Hilliard/Navier-Stokes system with 3D flows.

Paper 4. Multicomponent and multiphase modeling and simulation of reactive wetting.

We have developed a multicomponent and multiphase model with fluid motion. The model is used to study reactive wetting in the case where concentration change of the spreading liquid and the substrate occurs. The model is based on a Gibbs energy functional of a given system. The governing equations consist of convective concentration and phase-field equations which are coupled to the Navier-Stokes equations with surface tension forces. Arbitrary phase diagrams, surface energies, and typical dimensionless numbers are some input parameters into the model. An axisymmetric model with an adaptive finite element method is utilized. Numerical simulations were done revealing two stages in the wetting process. First, the

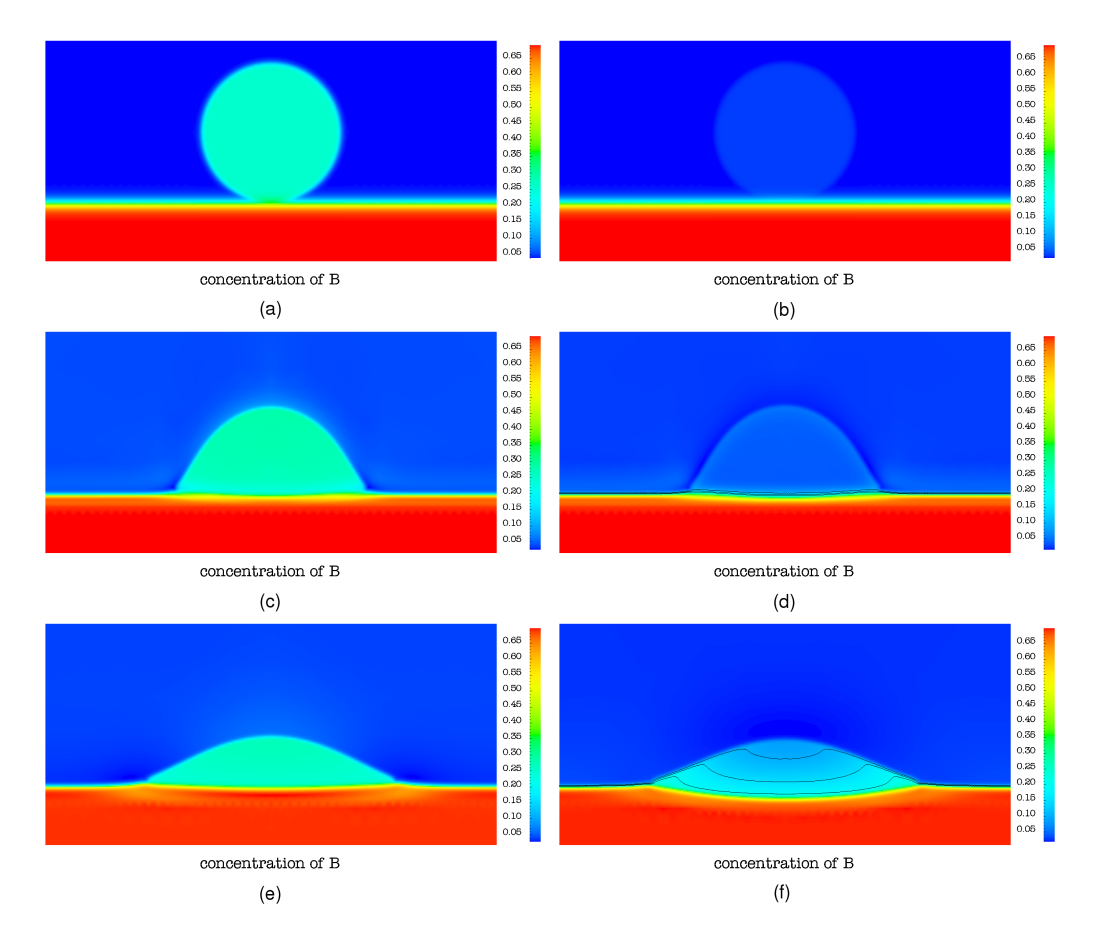


FIGURE 5.6. Concentration profiles of the B-atoms for nonreactive and reactive (b-d-f) at nondimensional times t=0,10, and 175, respectively. Isolines are plotted in (d) and (f) with B-isoconcentrates 0.10, 0.15, and 0.20 (top to bottom).

convection-dominated stage where rapid spreading occurs. The dynamics of the wetting is found to match with a known hydrodynamic theory for spreading liquids. Second, the diffusion-dominated stage where we observed depression of the substrate-liquid interface and elevation of the contact line region.

Figure 5.6 shows the concentration profiles of B-atoms for two cases with non-reactive and reactive case. The maximum concentration is 0.65 which is in the substrate in all cases. With nonreactive (Fig. 5.6a), the concentration of B starts with 0.26 in the spreading liquid compared to a much smaller value of 0.03 in the OIC case (Fig. 5.6b). In the succeeding Figures 5.6d and 5.6f, we see the transport of B-atoms into the spreading liquid while no observable change in B-concentration with the nonreactive case. This draws us to the conclusion that the transport of atoms across the interface changes the bulk energies causing the depression of the substrate-liquid interface.

Paper 5. Multicomponent and multiphase simulations of liquid phase sintering.

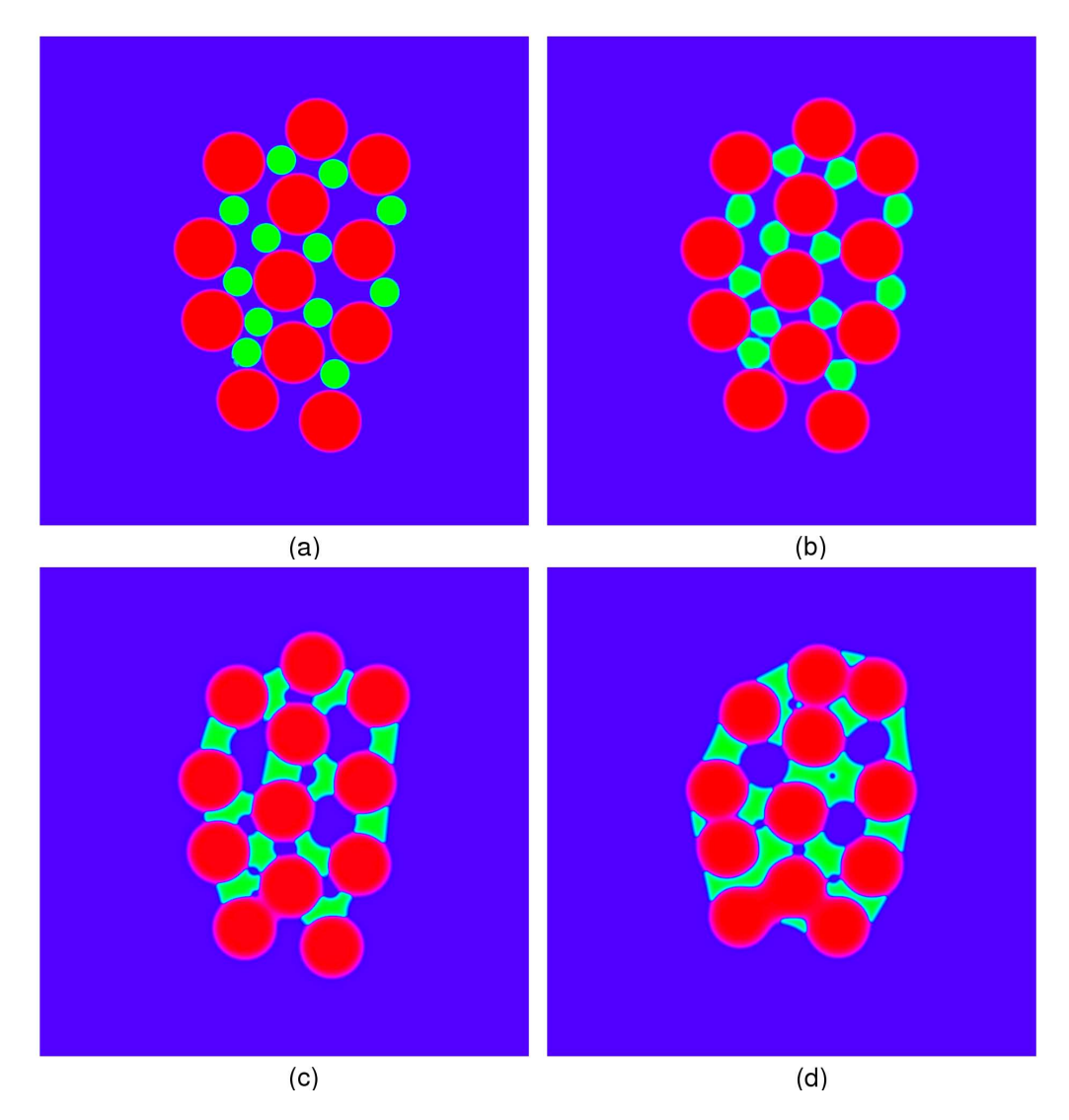


FIGURE 5.7. The evolution of the microstructure during liquid phase sintering with a metastable equilibrium contact angle $\theta_m = 36^{\circ}$ at dimensionless time t = 0, 2, 20, 100, respectively.

Using the general model presented in Paper 4, numerical simulations of liquid phase sintering are presented. Important dynamics in liquid phase sintering such as rapid wetting and motion of particles due to capillarity are studied. Some factors that are known to significantly affect the dynamics of the sintering process such as contact angles and volume ratios are investigated. Comparison with existing theories on the motion of particles in liquid phase sintering is also discussed.

5. SUMMARY OF RESULTS

In Fig. 5.7a, twelve liquid drops distributed over a matrix of twelve spherical solid particles of equal sizes is shown. The size of the liquid drops are smaller than the solid particles. In Fig. 5.7b, the liquid drops rapidly wet the solid grains. Then in Fig. 5.7c, more spreading is observed and at this time coalescence between liquid drops occurs and also the joining of two solid grains upon contact. In Fig. 5.7d, due to capillary forces the compact undergoes rearrangement in which more coalescences and pore shrinkage/elimination occur.

CHAPTER 6

Conclusions and outlook

The diffuse-interface models that are presented in this thesis for binary and ternary systems are based on the free energy of the system and they are often referred to as phase-field based models. Basically, the free energy of a given system is the sum of all bulk, gradient, and wall energies. Starting from the free energy, the derivation of phase-field based models follows from basic laws of thermodynamics. Thus, the governing equations are expected to point toward the right physics.

The binary model, more specifically the coupled Navier-Stokes/Cahn-Hilliard equations, was used to study different two-phase flows including problems related to microfluidics. Numerical issues using this model have also been addressed such as the need for mesh adaptivity and time-step restrictions. Moreover, the flexibility of this model to simulate 2D, axisymmetric, and 3D flows has been demonstrated. In addition, agreement with theory and experiments has been established.

The ternary model, on the other hand, is developed for more complicated flows such as liquid phase sintering. Detailed analysis of the dynamics involved during liquid phase sintering is shown. In particular, reactive and nonreactive wetting and the motion of particles due to capillarity are investigated.

The long term goal for modeling and simulation of liquid phase sintering is that, given the real parameters of the materials involved, one should be able to simulate and directly observe the evolution of the microstructure during the sintering process as if the experiment is being done. The simulations will not just reveal the underlying mechanisms at the microlevel but also provide densification rates, final shape after shrinkage/expansion, existence of cracks, sizes of pores, etc. In addition, the manipulation of the control parameters can also assist in creating new types of materials before the actual experiment or testing is done. It may still be a long way to go but the mathematical model presented here is geared towards the realisation of the abovementioned goal.

Many interesting problems in two-phase flows still remain elusive, at least from a computational point of view. The effects of surface roughness such as hysteresis are common in many applications. Similarly, the effects of surface-active materials or surfactants are either destructive or constructive depending on the application. Electrowetting is also an interesting computational problem since there are still many intricacies observed at or near the wetting line that requires analysis (Quilliet & Berge 2001). The process of boiling is a common phenomena that still puzzles many scientists. It would be interesting to see how a bubble grows from a nucleation site and investigate the factors affecting bubble size before departure and frequency of generation.

28 6. CONCLUSIONS AND OUTLOOK

A computational framework for these problems requires a basic description of the interface, for instance a diffuse-interface model; an equation that governs the motion of fluid, such as the Navier-Stokes equations; and the inclusion of additional effect/s, for instance in the boiling problem discussed above the heat equation can be included and coupled to the other governing equations. Then possibly one can identify factors that affect the process under study, identify thresholds for reproducibility, or effectively incorporate or isolate different physical effects into or from a model for different case studies.

Modeling and simulations of capillary phenomena can be viewed as a way to understand capillary effects and its intricacies, and also effectively explore areas or problems where theory and experiments have their limitations.

Acknowledgment

I am gratefully indebted to my supervisor, Prof. Gustav Amberg, whose knowledge, experience, and cunning ability to make one understand the basic principles of science are truly remarkable. His innate 'engineering' ability that never runs out of ideas on how to make things work is equally impressive. On the lighter side, having spent some time with him sailing, skiing, and discussing mundane matters was joyfully rewarding.

Along the way I have been influenced and have learned from other people's knowledge, way of thinking, and insights on many different subject areas. My special thanks is extended to my collaborators, Dr. Minh Do-Quang for many interesting discussions, scientific and non, Klara Grönhagen for being my materials science consultant, Prof. John Ågren for meticulously examining our manuscripts, Dr. Johan Sjödahl, Dr. Mårten Stjernström, Prof. Johan Roeraade, and Dr. Irina Singer-Loginova. I also appreciate the discussions I had with the members of the Computational Phase Transformation Group especially Prof. Anders Szepessy, Prof. Gunilla Kreiss, Elin Olsson, Erik von Schwerin, Dr. Mattias Sandberg and Dr. Henrik Strandlund. A correspondence with Dr. David Jacqmin during my first year of studies was also helpful.

The high level of scientific activity as well as the friendly atmosphere at the Department of Mechanics, Royal Institute of Technology (KTH), has also been a driving force that kept me going until the finish line. My sincere thanks to the staff, colleagues, and friends at the department, especially Yuan Lin, Tobias Strömgren, Ramis Örlu, Darja Ljubimova, Kazuya Goto, Veronica Eliasson, Dr. Junichiro Shiomi, Dr. Olivier Macchion, Dr. Astrid Herbst, Dr. Nulifer Ipek, Dr. Jérôme Hæpffner, Jordan Ko, Ingunn Wester, Bubba Darbo, and Pär Ekstrand.

The financial support from the Swedish Foundation for Strategic Research (SSF) and the computing resources from the Swedish National Infrastructure for Computing (SNIC) and the Center for Parallel Computers (PDC), KTH are highly appreciated.

I am very thankful for the unconditional support and encouragement from my family, especially my mother Lining, and my friends especially Ian Agulo, Rodolfo and Rose Manalili, Jonathan Esguerra, Christopher Caligagan, and the rest of Göteborg and Stockholm friends. My son Karl Vincent deserves a special mention for my renewed perspective on life. Finally, a heartfelt thanks to my loving wife Chriz for proofreading some parts of this thesis, for many articulative discussions, and for more than a decade pile of treasured moments. *Iddu ta ka, Mahal.*

Bibliography

- Addamson, A.W. 1990 *Physical Chemistry of Surfaces*, 5th edn. New York: John Wiley & Sons, Inc.
- Amberg, G., Tönhardt, R. & Winkler, C. 1999 Finite element simulations using symbolic computing. *Math. & Comp. in Sim.* 49, 257–274.
- ANDERSON, D.M., McFadden, G.B. & Wheeler, A.A. 1998 Diffuse-interface methods in fluid mechanics. *Annu. Rev. Fluid Mech.* **30**, 139–165.
- Anestiev, L.A. & Froyen, L. 1999 Model of the primary rearrangement processes at liquid phase sintering and selective laser sintering due to biparticle interactions. *J. Appl. Phys.* 86, 4008–4017.
- Badalassi, V.E., Ceniceros, H.D. & Banerjee, S. 2003 Computation of multiphase systems with phase field models. *J. Comp. Phys.* **190**, 371–397.
- BARRETT, J.W. & BLOWEY, J.F. 1995 An error bound for the finite element approximation of the Cahn-Hilliard equation with logarithmic free energy. *Numer. Math.* 72, 1–20.
- BARRETT, J.W. & BLOWEY, J.F. 1999 Finite element approximation of the Cahn-Hilliard equation with concentration dependent mobility. *Math. Comp.* **68**, 487–517.
- BARRETT, J.W. & BLOWEY, J.F. 2002 Finite element approximation of an Allen-Cahn-Hilliard equation. *IMA J. Numer. Ana.* 22, 11–71.
- BATES, P.W. & FIFE, P.C. 1993 The dynamics of nucleation for the Cahn-Hilliard equation. SIAM J. Appl. Maths 53, 990–1008.
- BECKER, R. & RANNACHER, R. 2001 An optimal control approach to a posteriori error estimation in finite element methods. *Acta Numerica* **10**, 1–102.
- Berg, J.C., ed. 1993 Wettability. Marcel Dekker, Inc.
- BOETTINGER, W.J., WARREN, J.A., BECKERMANN, C. & KARMA, A. 2002 Phase-field simulations of solidification. *Ann. Rev. Mater. Res.* **32**, 163–194.
- Braun, R.J., Murray, B.T. & Soto, J., Jr. 1997 Adaptive finite-difference computations of dendritic growth using a phase-field model. *Modelling Simul. Mater. Sci. Eng.* 5, 365–380.
- BROCHARD, F. 1989 Motion of droplets on solid surfaces induced by chemical and temperature gradients. *Langmuir* 5, 432–438.
- Burns, M.A., Johnson, B.N., Brahmasandra, S.N., Handique, K., Webster, J.R., Krishnan, M., Sammarco, T.S., Man, P.M., Jones, D., Heldsinger, D., Mastrangelo, C.H. & Burke, D.T. 1998 An integrated nanoliter dna analysis device. *Science* 282, 484–487.
- Cahn, J.W. 1961 On spinodal decomposition. Acta Metallurgica 9, 795–801.

- Chen, L.Q. 2002 Phase-field models for microstructural evolution. *Ann. Rev. Mater.* Res. 32, 113–140.
- CONINCK, J.D., D'ORTONA, U., KOPLIK, J. & BANAVAR, J.R. 1995 Terraced spreading of chain molecules via molecular dynamics. *Phys. Rev. Lett.* **74**, 928–931.
- Cox, R.G. 1986 The dynamic of the spreading of liquids on a solid surface. Part 1. Viscous flow. J. Fluid Mech 168, 169–194.
- Debnath, L. & Mikusinski, P. 1999 Introduction to Hilbert spaces with applications, 2nd edn. Academic Press.
- Do-Quang, M., Villanueva, W., Singer-Loginova, I. & Amberg, G. 2007 Parallel adaptive computation of some time-dependent materials-related microstructural problems. *Bull. Pol. Acad. Sci.* To appear.
- Dussan, E.B. 1979 On the spreading of liquids on solid surfaces: Static and dynamic contact lines. *Ann. Rev. Fluid Mech.* 11, 371–400.
- Dussan, E.B. & Davis, S.H. 1974 On the motion of a fluid-fluid interface along a solid surface. *J. Fluid Mech.* **65**, 71–95.
- ELLIOTT, C.M. & LARSSON, S. 1992 Error estimates with smooth and nonsmooth data for a finite element method for the Cahn-Hilliard equation. *Math. Comp.* **58**, 603–630.
- ERIKSSON, K., ESTEP, D., HANSBO, P. & JOHNSON, C. 1995 Introduction to adaptive methods for partial differential equations. *Acta Numerica* pp. 105–158.
- ERIKSSON, K., ESTEP, D., HANSBO, P. & JOHNSON, C. 1996 Computational Differential Equations. Lund, Sweden: Studentliteratur.
- EVANS, L.C. 1998 Partial Differential Equations, Graduate Studies in Mathematics, vol. 19. Amer. Math. Soc.
- Fan, C.F. & Cagin, T. 1995 Wetting of crystalline polymer surfaces: A molecular dynamics simulation. *J. Chem. Phys.* **103**, 9053–9061.
- Garcke, H., Rumpf, M. & Weikard, U. 2001 The Cahn-Hilliard equation with elasticity finite element approximation and qualitative studies. *Interfaces and Free Boundaries* 3, 101–118.
- DE GENNES, P.G. 1992 Simple views on condensed matter, pp. 289–326. World Scientific Publishing Co. Pte. Ltd.
- DE GENNES, P.G., BROCHARD-WYART, F. & Quéré, D. 2004 Capillarity and Wetting Phenomena. Springer-Verlag, N.Y., Inc.
- German, R. 1985 Liquid phase sintering. Plenum Press, N.Y.
- Gresho, P.M. & Sani, R.L. 1998 Incompressible flow and the finite element method. New York: John Wiley & Sons, Inc.
- Guermond, J.L., Miney, P. & Shen, J. 2006 An overview of projection methods for incompressible flows. *Comput. Methods Appl. Mech. Engrg.* **195**, 6011–6045.
- Guermond, J.L. & Quartapelle, L. 1998 On stability and convergence of projection methods based on pressure Poisson equation. *Int. J. Numer. Methods Fluids* **26**, 1039–1053.
- Hansbo, P. & Szepessy, A. 1990 A velocity-pressure streamline diffusion finite element method for the incompressible Navier-Stokes equations. *Comput. Meth. Appl. Mech. and Eng.* 84, 175–192.
- HEADY, R.B. & CAHN, J.W. 1970 An analysis of the capillary forces in liquid phase sintering of spherical particles. *Metallurgical Trans.* 1, 185–189.

- HIRT, C.W. & NICHOLS, B.D. 1981 Volume of fluid (VOF) method for the dynamics of free boundaries. *J. Comp. Phys.* **39**, 201–225.
- HOCKING, L.M. & RIVERS, A.D. 1982 The spreading of a drop by capillary action. *J. Fluid Mech.* **121**, 425–442.
- HOFFMAN, J. 2002 Computational modeling of complex flows. PhD thesis, Chalmers University of Technology, Sweden.
- HOFFMAN, R. 1975 A study of the advancing interface. J. Colloid and Interface Science **50**, 228–241.
- HUGHES, T.J.R., FRANCA, L.P. & BALESTRA, M. 1986 A new finite element formulation for computational fluid dynamics: V. Circumventing the Babuska-Brezzi condition: A stable Petrov-Galerkin formulation for the Stokes problem accommodating equal order interpolations. Comput. Methods Appl. Mech. Engrg. 59, 85–99.
- Huh, C. & Scriven, L.E. 1971 Hydrodynamic model of steady movement of a solid/liquid/fluid contact line. *J. Colloid Interface Sci.* **35**, 85–101.
- Huppmann, W.J. & Riegger, H. 1975 Modeling of rearrangement processes in liquid phase sintering. *Acta Metallurgica* **23**, 965–971.
- ICHIMURA, K., OH, S.-K. & NAKAGAWA, M. 2000 Light-driven motion of liquids on a photoresponsive surface. *Science* **288**, 1624–1626.
- ISRAELACHVILI, J. 1992 Intermolecular and surface forces. San Diego, CA: Academic Press Inc.
- JACQMIN, D. 1999 Calculation of two-phase Navier-Stokes flows using phase-field modeling. *J. Comput. Phys.* **155**, 96–127.
- Jacqmin, D. 2000 Contact-line dynamics of a diffuse fluid interface. *J. Fluid Mech.* **402**, 57–88.
- Jiang, J.-S., Oh, S.-G. & Slattery, J. 1979 Correlation for dynamic contact angle. J. Coll. Inter. Sci. 69, 74–77.
- JIN, W., KOPLIK, J. & BANAVAR, J.R. 1997 Wetting hysteresis at the molecular scale. *Phys. Rev. Lett.* **78**, 1520–1523.
- JOHNSON, R.E., Jr. & DETTRE, R.H. 1964 Contact angle hysteresis. III. Study of idealized heterogenous surface. J. Phys. Chem. 68, 1744–1750.
- KARNIADAKIS, G., BESKOK, A. & ALURU, N. 2005 Microflows and Nanoflows: Fundamentals and Simulation, Interdisciplinary Applied Mathematics, vol. 29. New York: Springer Science+Business Media, Inc.
- Kim, J., Kang, K. & Lowengrub, J. 2004 Conservative multigrid methods for Cahn-Hilliard fluids. *J. Comput. Phys.* **193**, 511–543.
- KINGERY, W.D. 1959 Densification during sintering in the presence of a liquid phase. I. Theory. J. Appl. Phys. 30, 301–306.
- KISTLER, S.F. 1993 Hydrodynamics of wetting. In *Wettability* (ed. J.C. Berg), *Surfactant Science Series*, vol. 49, pp. 311–429. New York: Marcel Dekker, Inc.
- LARSSON, S. & THOMÉE, V. 2003 Partial differential equations with numerical methods. Springer New York, Inc.
- LASZLOFFY, A., LONG, J. & PATRA, A. 2000 Simple data management, scheduling and solution strategies for managing the irregularities in parallel adaptive *hp* finite element simulations. *Parallel Computing* **26**, 1765–1788.
- LEE, S.-M., CHAIX, J.-M., MARTIN, C.L., ALLIBERT, C.H. & KANG, S.L. 1999

- Computer simulation of particle rearrangement in the presence of liquid. *Metals and Materials* 5, 197–203.
- LEE, S.-M. & KANG, S.L. 1997 Theoretical analysis of liquid-phase sintering: Pore filling theory. *Acta Materialia* 46, 3191–3202.
- Lesage, A-C., Allain, O. & Dervieux, A. 2007 On level set modeling of bi-fluid capillary flow. *Int. J. Num. Meth. Fluids* **53**, 1297–1314.
- LIU, R.H., STREMLER, M.A., SHARP, K.V., OLSEN, M.G., SANTIAGO, J.G., ADRIAN, R.J., AREF, H. & BEEBE, D.J. 2000 Passive mixing in a three-dimensional serpentine microchannel. *J. Microelectromechanical Systems* **9**, 190–197.
- LOGINOVA, I., ÅGREN, J. & AMBERG, G. 2003 The phase-field approach and solute drag modeling of the transition to massive $\gamma \to \alpha$ transformation in binary Fe-C alloys. *Acta Materialia* **51**, 1327–1339.
- MOTTA, F.V., BALESTRA, R.M., RIBEIRO, S. & TAGUCHI, S.P. 2004 Wetting behaviour of SiC ceramics, Part I. *Materials Letters* **58**, 2805–2809.
- Mukherjee, A. & Kandlikar, S.G. 2007 Numerical study of single bubbles with dynamic contact angle during nucleate pool boiling. *Int. J. Heat Mass Transfer* **50**, 127–138.
- Murray, B.T., Wheeler, A.A. & Glicksman, M.E. 1995 Simulations of experimentally observed dendritic growth behavior using a phase-field model. *J. Crystal Growth* 154, 386–400.
- OLEVSKY, E.A. 1998 Theory of sintering: from discrete to continuum. *Materials Sci.* and Engrg. 23, 41–100.
- Olsson, E. & Kreiss, G. 2005 A conservative level set method for two phase flow. *J. Comp. Phys.* **210**, 225–246.
- PROBSTEIN, R.F. 2003 Physicochemical Hydrodynamics: An Introduction, 2nd edn. John Wiley & Sons, Inc.
- Quilliet, C. & Berge, B. 2001 Electrowetting: a recent outbreak. Curr. Opin. Coll. Int. Sci. 6, 34–39.
- RIVARA, M.C. 1989 Selective refinement/derefinement algorithms for sequences of nested triangulations. *Int. J. Numer. Meth. Eng.* 28, 2889–2906.
- ROWLINSON, J.S. & WIDOM, B. 1982 Molecular theory of capillarity. New York: Oxford University Press.
- SAAD, Y. 1996 Iterative methods for Sparse Linear Systems. Boston, MA: PWS Publishing Company.
- SCHMID, P.J. & HENNINGSON, D.S 2001 Stability and Transition in Shear Flows, Applied mathematical sciences, vol. 142. Springer-Verlag N.Y., Inc.
- SEPPECHER, P. 1996 Moving contact lines in the Cahn-Hilliard theory. *Int. J. Engng. Sci.* **34**, 977–992.
- SINGH, P. & JOSEPH, D.D. 2005 Fluid dynamics of floating particles. *J. Fluid Mech.* 530, 31–80.
- Son, G. & Hur, N 2002 A coupled level set and volume-of-fluid method for the boyancy-driven motion of fluid particles. *Num. Heat Transfer, Part B* **42**, 523–542.
- Son, G. & Hur, N 2007 A level set formulation for incompressible two-phase flows on nonorthogonal grids. *Num. Heat Transfer*, *Part B* **48**, 303–316.
- Squires, T.M. & Quake, S.R. 2005 Microfluidics: Fluid physics at the nanoliter scale. *Rev. Mod. Phys.* **77**, 977–1026.

- STROOCK, A.D., DERTINGER, S.K., AJDARI, A., MEZIC, I., STONE, H.A. & WHITE-SIDES, G.M. 2002 Chaotic mixer for microchannels. *Science*.
- Sussman, M., Smereka, P. & Osher, S. 1994 A level set approach for computing solutions to incompressible two-phase flow. *J. Comp. Phys.* **114**, 146–159.
- SVOBODA, J., RIEDEL, H. & GAEBEL, R. 1995 A model for liquid phase sintering. *Acta. Materialia* 44, 3215–3226.
- Tabeling, P. 2005 Introduction to Microfluidics. New York: Oxford University Press Inc.
- TAGUCHI, S.P., MOTTA, F.V., BALESTRA, R.M. & RIBEIRO, S. 2004 Wetting behaviour of SiC ceramics, Part II. *Materials Letters* **58**, 2810–2814.
- TANNER, L.H. 1979 The spreading of silicone oil drops on horizontal surfaces. J. Phys. D: Appl. Phys. 12, 1473–1484.
- THORSEN, T., ROBERTS, R.W, ARNOLD, F.H. & QUAKE, S.R. 2001 Dynamic pattern formation in a vesicle-generating microfluidic device. *Phys. Rev. Lett.* **86**, 4163–4166.
- UNVERDI, S.O. & TRYGGVASON, G. 1992 A front-tracking method for viscous, incompressible, multi-fluid flows. *J. Comp. Phys.* **100**, 25–37.
- UPADHAYAYA, G.S. 2000 Sintered Metallic and Ceramic Materials. England: Jon Wiley & Sons Ltd.
- VILLANUEVA, W. & Amberg, G. 2006 Some generic capillary-driven flows. *Int. J. Multiphase Flow.* **32**, 1072–1086.
- VILLANUEVA, W., SJÖDAHL, J., STJERNSTRÖM, M., ROERAADE, J. & AMBERG, G. 2007 Microdroplet deposition under a liquid medium. *Langmuir* 23, 1171–1177.
- Voinov, O.V. 1976 Hydrodynamics of wetting. Fluid Dyn. 11, 714–721.
- VAN DER WAALS, J.D. 1893 The thermodynamic theory of capillarity under the hypothesis of a continuous variation of density. *Verhandel. Konink. Akad. Weten.* 1, english translation in *J. Stat. Phys.* 20 (1979).
- Warren, J.A. & Boettinger, W.J. 1994 Prediction of dendritic growth and microsegregation patterns in a binary alloy using the phase-field method. *Acta metall.* mater. 43, 689–703.
- Wheeler, A.A., Murray, B.T. & Schaefer, R.J. 1993 Computation of dendrites using a phase field model. *Physica D* **66**, 243–262.
- Yang, J., Koplik, J. & Banavar, J.R. 1991 Molecular dynamics of drop spreading on a solid surface. *Phys. Rev. Lett.* **67**, 3539–3542.
- Young, T. 1805 An essay on the cohesion of fluids. *Philos. Trans. Soc. London* **95**, 65–87
- ZISMAN, W.A. 1964 Contact angles, wettability and adhesion. In *Advances in Chemistry Series 43* (ed. F.M. Fowkes), p. 1. Washington, D.C.: Amer. Chem. Soc.

Part 2

Papers